Augmenting sensitivity of surface plasmon resonance (SPR) sensors with the aid of anti-reflective coatings (ARCs)

Das Cm, Ouyang Ql, Kang Lx, Guo Y, Dinh Xq, P. Coquet, Yong Kt

Augmenting Sensitivity of Surface Plasmon Resonance (SPR) Sensors with the Aid of Anti-reflective Coatings (ARCs).

Chandreyee Manas Das[1,2], Qingling Ouyang[1,2], Lixing Kang[1,2], Yan Guo[1], Xuan-Quyen Dinh[1], Philippe Coquet[1,3] and Ken-Tye Yong[1,2,*]

1 CINTRA CNRS/NTU/THALES, UMI 3288, Research Techno Plaza, 50 Nanyang Drive, Border X Block, Singapore 637553
2 School of Electrical and Electronic Engineering, Nanyang Technological University, Singapore
3 Institut d'Electronique, de Microélectronique et de Nanotechnologie (IEMN), CNRS UMR 8520 – Université de Lille 1, 59650 Villeneuve d'Ascq, France
Corresponding Author
* E-Mail: ktyong@ntu.edu.sg

***Abstract*— Surface plasmon resonance (SPR)-based biosensors are an integral and indispensable aspect of present-day pathology, owing to its efficient real-time and label-free detection capabilities. Enhancing the sensitivity of these sensors is of paramount importance as it indirectly affects the detection limits of biomolecules. In this simulation work, we make use of antireflective coatings (ARCs) (double and multi-layered), made up of nanomaterials with alternating high and low refractive indices (R.I.) (TiO_2/SiO_2, TiO_2/MgF_2, Nb_2O_5/SiO_2 and Nb_2O_5/MgF_2); to enhance the sensitivity of Si-Transition Metal Dichalcogenides (TMDCs)-based SPR sensors. To summarize the entire outcome, our simulation predicts the sensitivity of the TiO_2-SiO_2-Au-Si-TMDC configuration to be 284 degRIU-1 at 633 nm of incident light wavelength.**

***Keywords*— Surface Plasmon Resonance, Biomolecular Detection, Sensitivity Enhancement, Anti-Reflective Coatings, Simulation and Modeling.**

1. Introduction

The electromagnetic (EM) light waves are present everywhere around us and it can give rise to many spectacular optical phenomena, one of them being the surface plasmon resonance. SPR is a surface phenomenon, where the interaction between the incident p-polarized light wave and the free electrons residing at the metal-dielectric surface, leads to the production of oscillatory surface plasmon waves (SPW) [1-3]. The resonance condition occurs when there is a matching of the propagation constants of the incident EM light wave and the SPW. Since this matching is immensely dependent on the physical characteristics of the analyte layer, even a slight change in its biochemical constituency will result in a detectable change in the physical sensing parameter like the SPR angle [4]. A change in the SPR output (optical) signal indicates a change in the refractive index (R.I.) of the analyte, which usually occurs beacause of the presence of biomolecules. Thus, SPR-based biological sensing is a highly sophisticated technique that calls for a multi-disciplinary approach involving specialized skills from nanofabrication, optical engineering and even medical sciences.

SPR sensing technology is being utilized in a wide variety of fields, like pathology, food safety and even environmental monitoring. The plasmonic testing scheme can surpass the benefits offered by other technologies like polymerase-chain reaction (PCR) and Enzyme linked immunosorbent assay (ELISA) [5]. In addition to the known features of SPR sensing, it can also offer high selectivity in terms of its pathogen detection capabilities. The plasmonic bio-sensing platform can serve as an important detection tool for the early diagnosis of malignant diseases like the detection of HeLa cells using biomarker Rhodamine 6G [6].

Even food and agriculture sectors can utilize the SPR sensing technique for detecting the concentration of Napropamide, a common herbicide used by farmers [7]. Moreover, biologists and researchers from the drug industry can also utilize SPR-based imaging systems to monitor important intracellular activities like the movement of protein kinase C (PKC) from the cytosol to the plasma membrane [8].

The addition of dielectric materials in the standard Kretschmann configuration enhances photon absorption that further promotes excitation of more surface plasmons resulting in an increase in sensitivity. Transition-metal di-chalcogenides (TMDCs) are a new class of 2D materials that are exquisitely known as "beyond graphene". The general notation of these materials is MX_2, where M is a transition metal like Tungsten (W) and Molybdenum (Mo) and X is an element from the chalcogen family like Sulphur (S), Selenium (Se) or Tellurium (Te). When the thickness of the TMDC layer is brought down to the nano scale, there is a drastic change in its atomic structure that results in a change in its optical property. For instance, due to quantum confinement, bulk MoS_2 having an indirect bandgap of 1.2 eV is transformed to nano scaled MoS_2 with a direct bandgap of 1.8 eV. This unique feature allows MoS_2 to be easily excited by external photons. TMDC based-SPR sensors have thus been able to provide a pronounced increase in sensitivity. In this work, we evaluate the role of Anti-Reflective Coatings, ARCs, in further enhancing the sensitivity of these TMDC sensors [9].

The efficiency of optoelectronic devices like photovoltaic devices (solar cells), organic LEDs (OLEDs) and optical instruments like telescopes and microscopes depends on the amount of incident light passing through these devices [10-14]. Conventional arrangement of photonic layers causes a high percentage of reflection loss, resulting in reduced efficiency. Anti-reflective coatings (ARCs) are nano-engineered structural modifications specifically designed to alter the optical light trapping capability of the photonic devices. An abrupt change of refractive index from the surrounding medium to the substrate causes a high amount of reflection loss. Anti-reflective coatings of sub-wavelength dimensions (generally of the order of few to several hundreds of nanometers), with refractive indices in between that of the substrate and the environment, can bring down the reflectvity, leading to a major improvement in efficiency. Stacking intermediate layers results in destructive interference of the reflected waves emerging out from the boundaries of different layers, which lead to a net cancellation of the reflected light and thus a reduced reflectance. Double and multi-layered ARCs are more common than single layered ones as they provide a broadband reduction in reflectivity, generally over the entire visible spectrum of EM light wave. These are predominantly made up of nano layers of alternating high and low refractive index (R.I.) materials like TiO_2/Nb_2O_5 (high R.I.) and MgF_2/SiO_2 (low R.I.) [15]. TiO_2 and SiO_2 are the two most common nano materials used as an ARC and these have been extensively used for the enhancement of performance of photovoltaic cells [16]. Additionally, Nb_2O_5 and MgF_2 films are recently explored materials that possess high transmittivity over the entire range of visible spectrum and thus these can be good additions to the family of ARCs [17-20]. In the SPR arrangement, the anti-reflection coating allows more incident light to get trapped and thus more surface plasmons at the metal-dielectric interface are excited. Since most of the incident energy is transferred in exciting more surface plasmons, the reflected light has a lower reflectivity and hence greater sensitivity can be realized [21].

The SPR curve of Ag has a sharper dip as compared to that of Au. Additionally, the sensitivity of Ag nanorods (NRs) is twice that of Au NRs in the visible spectrum range of 600-700 nm. However, Ag is not chemically stable as it is prone to oxidation. Plasmonic noble metals like Au and Ag embedded in metal oxides have been used in increasing the response and sensitivity of gas sensors. Inclusion of nanoparticles of noble metals (Au and Ag) in TiO_2 mesoporous structure results in enhanced photon absorption of dye-sensitized solar cells (DSSC). The generation of surface plasmons by nano sized noble metals have a positive effect on the photocurrents and power conversion efficiencies (PECs) of optoelectronic devices. Thus, Gold (Au) and Silver (Ag) are the most preferred plasmonic metals for SPR applications. All metals have complex dielectric constants. Metals possessing larger negative real part and smaller positive imaginary part have good plasmonic effects. Other non-noble metals like Copper (Cu) and Aluminium (Al) also fulfill these conditions, and hence these can also be used as plasmonic metals in the SPR arrangement. Thus, in this work we present a comprehensive analysis using these four plasmonic metals. In the upcoming remaining part of the paper, we present the sensor structure along with the necessary mathematical equations, used in the simulations, in Section II. Section III deals with the modeling and

simulation results for the proposed structure. In Section IV, we compare the sensitivity of our structure with other reported works. Finally, we end the paper with concluding remarks in Section V.

2. Simulation Method

2.1 Sensor Structural Configuration

The sensor configuration has been depicted in Figure 1. In brief, there are seven layers starting from the SF-10 prism at the bottom and ending with the analyte layer at the top. The anti-reflective coatings (TiO_2-SiO_2, TiO_2-MgF_2, Nb_2O_5-SiO_2 and Nb_2O_5-MgF_2) form the second and the third layers respectively. The plasmonic metal (Au, Ag, Cu and Al) forms the fourth layer followed by silicon (5th layer) and TMDC (WS_2, MoS_2, WSe_2, and $MoSe_2$) (6th layer). The analyte (de-ionized (D.I.) water) forms the last layer.

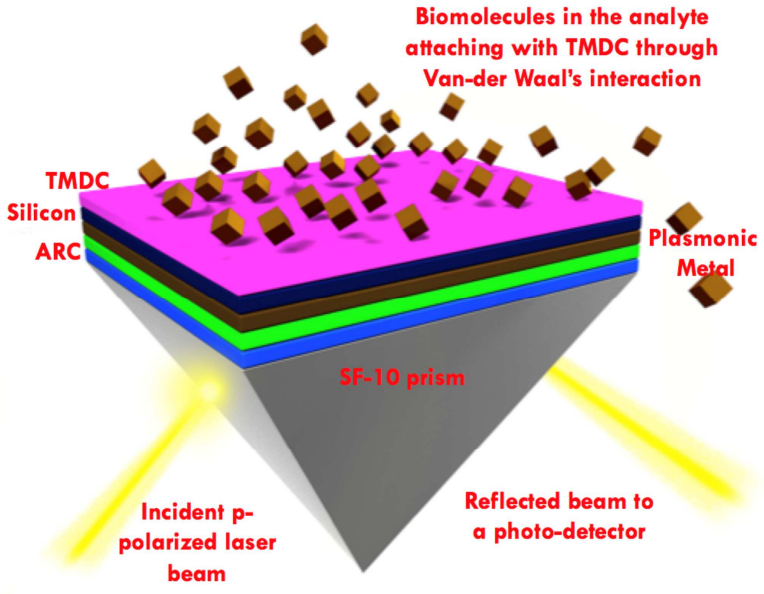

Fig. 1. Structure of the ARC modified Si-TMDC based SPR sensor

2.2. Fresnel's Equations

Since there are multiple layers involved in the SPR structure, we use Fresnel's Equations (Transfer Matrix Method) for calculating the reflectivity R [9].

$$M = \prod_{k=2}^{N-1} M_k \quad , \quad \text{where} \quad M_k = \begin{bmatrix} \cos\beta_k & \frac{-i\sin\beta_k}{q_k} \\ -iq_k\sin\beta_k & \cos\beta_k \end{bmatrix} \tag{1}$$

$$q_k = \frac{(\varepsilon_k - {n_1}^2 \sin^2\theta_1)^{\frac{1}{2}}}{\varepsilon_k} \tag{2}$$

$$\beta_k = \frac{2\pi d_k}{\lambda}\left((\varepsilon_k - {n_1}^2 \sin^2\theta_1)\right)^{\frac{1}{2}} \tag{3}$$

$$r_p = \frac{(M_{11}+M_{12}q_N)q_1-(M_{21}+M_{22}q_N)}{(M_{11}+M_{12}q_N)q_1+(M_{21}+M_{22}q_N)}$$
(4)

$$R_p = |r_p|^2$$
(5)

$$S = \frac{d\theta_{SPR}}{dn_{bio}}$$
(6).

Illuminating on the various variables in equation 1 through 6, N is the total number of layers. $\lambda = 633$ nm, is the wavelength of the incident light. n_k and ε_k denote the R.I. and dielectric constant of the k-th layer. Also, $\varepsilon_k = (n_k)^2$. d_k is the thickness of the k-th layer and θ_1 is the angle of incident p-polarized light. R_p is the reflectivity. θ_{SPR} is the angle of minimum reflectivity, n_{bio} is the R.I. of the analyte layer containing the bio-molecules and S is the angular sensitivity. M is the characteristic matrix of the N-layer model and it is the main matrix of the Transfer Matrix Method (TMM). As we use the angular interrogation method for the calculation of sensitivity, we observe the change in SPR angle (θ_{SPR}) for a small change in the R.I. of the analyte ($\Delta n_{bio} = 0.005$). The R.I. of SF-10 prism and silicon and the dielectric constants of the four TMDC materials can be found in [9]. The dielectric constants of the different plasmonic metals can be found using the Drude model [4]. The refractive indices of the four anti-reflective materials can be found in [22-25]. The R.I. of D.I. water is taken as 1.33. The thickness of the plasmonic metal layer is as follows: Au – 50 nm, Ag- 45 nm, Cu – 40 nm and Al – 25 nm. For Silicon, we take the thickness as 5 nm. For the TMDCs, the thickness of each layer is as follows: WS_2 – 0.8 nm, MoS_2 – 0.65 nm, WSe_2 – 0.7 nm and $MoSe_2$ – 0.7 nm. The thicknesses of all the layers are kept fixed except the TMDC layer where we vary the number of layers, N_{layer}, and obtain the optimized total thickness ($d_{TMDC} = N_{layer} \times t_{TMDC}$, t_{TMDC} is the thickness of a single layer and d_{TMDC} is the total thickness) that gives us maximum sensitivity.

3. Modeling and Simulation Results

3.1. Simulation Results

For the optimal functioning of solar cells, it is very necessary to ensure that most of the incident sunlight gets absorbed. Figure S1 in the supporting information shows our simulation results, where we demonstrate the role of ARCs in reducing the reflectivity of the substrate material. We evaluate the variation of reflectivity as the wavelength of the incident light varies in the visible spectrum. We observe that when we put intermediate layers of anti-reflective materials TiO_2 and SiO_2 in between air and Si substrate, there is a marked reduction in reflectivity. Six layers of anti-reflective materials consisting of alternating layers of TiO_2 and SiO_2 (i.e. 3 layers of double layered ARC) gives the minimum reflectivity as compared to other arrangements.

We perform the simulations at 633 nm for four ARC combinations TiO_2-SiO_2, TiO_2-MgF_2, Nb_2O_5-SiO_2 and Nb_2O_5-MgF_2, four TMDC materials WS_2, MoS_2, WSe_2 and $MoSe_2$ along with four plasmonic metals Au, Ag, Cu and Al and hence we have 64 different sensor arrangements. We start by optimizing the thickness of TiO_2 and SiO_2 layers. Figures S2 and S3 in the supporting information show the variation of minimum reflectivity and sensitivity as a function of thickness of TiO2 and SiO2. For optimization of TiO_2, SiO_2 is fixed at 20 nm, Au at 50 nm, Si at 5 nm, WS_2 at 0.8 nm, MoS_2 at 0.65 nm, WSe_2 at 0.7 nm and $MoSe_2$ at 0.7 nm. Similarly, for optimization of SiO_2, TiO_2 is fixed at 20 nm, Au at 50 nm, Si at 5 nm, WS_2 at 0.8 nm, MoS_2 at 0.65 nm, WSe_2 at 0.7 nm and $MoSe_2$ at 0.7 nm. We observe that for TiO_2, both the minimum reflectivity and sensitivity increase as a function of TiO_2 thickness and reach a peak value beyond which these values start to decline. Thus, for optimum thickness, we choose it at a value where the minimum reflectivity is relatively smaller and the sensitivity is relatively larger than at other values of thicknesses. And this value is 95 nm for TiO_2. At this thickness, the sensitivity is maximum for all TMDC materials and the minimum reflectivity is relatively smaller as compared to other thicknesses. For SiO_2, the trend is a bit different. The minimum reflectivity keeps on decreasing as a function of SiO_2 thickness and the sensitivity also follows an overall declining trend. Thus, it is not possible to choose a thickness corresponding to

smallest minimum reflectivity and largest sensitivity both at the same time. Hence, we go for a compromise and choose a thickness in the intermediate range, where the minimum reflectivity value is small (though not smallest) and the sensitivity is large (though not largest). And this value is 20 nm for SiO_2. We use the same thickness as arrived here for all other combinations of ARCs and plasmonic metals.

After arriving at the optimized thickness values, for every unique sensor arrangement (64 sensor configurations in total), we vary the number of TMDC layers (N_{layer}) to arrive at the best thickness value ($d_{TMDC} = N_{layer} \times t_{TMDC}$) that gives us the highest sensitivity. Figure 2 shows the simulation results for plasmonic metal Au and ARCs of TiO_2 and SiO_2. We observe a drop in minimum reflectivity and an increase in sensitivity as we increase the TMDC layers. This can be attributed to the fact that increased thickness of the dielectric material (TMDC), results in greater photon absorption. Thus, more energy is transferred to the free electrons on the plasmonic metal and hence more surface plasmons are produced that oscillate with greater amplitude during resonance giving a higher sensitivity. Figure S4 in supporting information presents the simulation results for all other 60 combinations.

a)

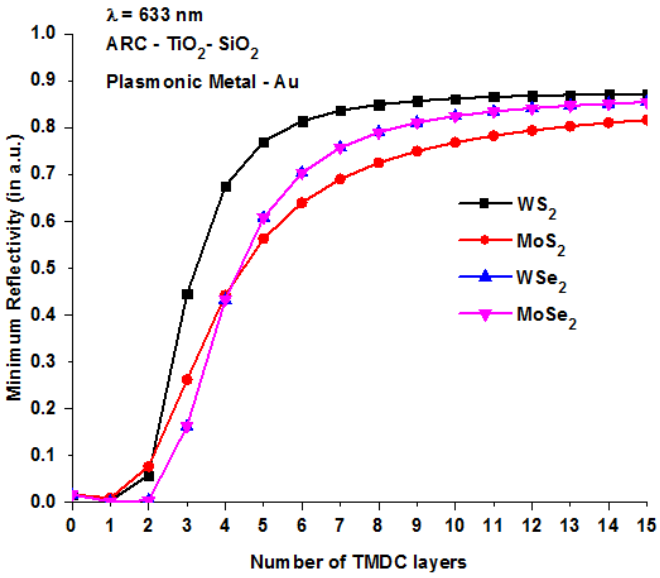

b)

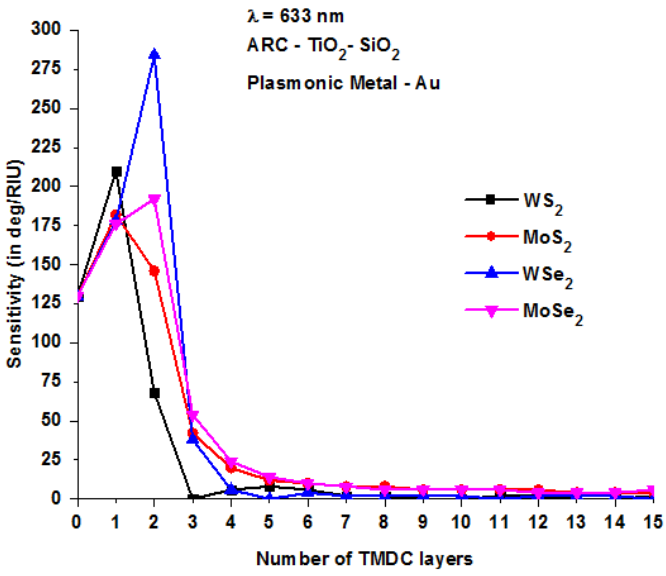

Figure 2a) Minimum Reflectivity and 2b) Sensitivity variation as a function of number of TMDC layers

Table 1 summarizes the outcome of the simulation results. Along with sensitivity, we also calculate Full-Width at Half Maximum (FWHM), Detection Accuracy (D.A.) and Quality Factor (Q). The DA or the signal-to-noise ratio (SNR) depends on how accurately and precisely, the sensor can detect changes in resonance angle or the change in refractive index of the sensing medium. It is defined as the ratio of change in resonance angle to the angular width of the SPR curve corresponding to 0.5 reflectance. Thus, the higher the DA or SNR, the better the sensor. This parameter is quite different from detection resolution or the limit of detection (LOD), which is the minimum concentration level of a chemical or a biomolecule that can be

S. No.	Plasmonic metal	ARC	TMDC	Initial SPR Angle	Final SPR Angle	Change in resonance angle ($d\theta_{SPR}$)	Sensitivity ($S = \frac{d\theta_{SPR}}{dn_{bio}}$)	FWHM	Detection Accuracy ($D.A. = \frac{d\theta_{SPR}}{FWHM}$)	Quality Factor ($Q = \frac{S}{FWHM}$)
1	Au	TiO_2-SiO_2	WSe_2 (2L)	74.55	75.97	1.42	284	22.79	0.062	12.46
2	Ag	TiO_2-SiO_2	WSe_2 (5L)	74.87	75.82	0.95	190	20.29	0.046	9.36
3	Cu	TiO_2-SiO_2	WSe_2 (6L)	74.54	75.61	1.07	214	21.43	0.049	9.98
4	Al	TiO_2-SiO_2	WS_2 (7L)	73.93	75.15	1.22	244	24.89	0.049	9.80

detected by the sensor. Thus, this is quite opposite to the DA or SNR. The lower the LOD, the better the sensor. With Au as the plasmonic metal and TiO_2-SiO_2 as the ARC and with 2 layers of WSe_2, we get the maximum sensitivity of 284 degRIU^{-1} at 633 nm of incident light. Additionally, we get a good detection accuracy of 0.062 along with a reasonable quality factor of 12.46. We can observe that as we change the plasmonic metal from Au to Al, we require greater number of TMDC layers to achieve higher sensitivity since the plasmonic efficiency of the metal decreases, and thus more light absorbing/transmitting layers of TMDC are required for compensation.

Table 1. Summary of simulation results at 633 nm ($\Delta n_{bio} = 0.005$)

Surface plasmon resonance is obtained at a particular angle of incidence where the intensity of the reflected light is minimum. Figure 3 shows the SPR curves for the four best arrangements highlighted in Table 1. As the angle of incidence is increased beyond the critical angle, we see a drop in reflectivity till it reaches the SPR angle, where the reflectivity is minimum. Beyond this angle, the reflectivity again starts to increase. We also present some additional simulation results in the supporting information. Figure S5 shows the variation of sensitivity as a function of the change in R.I. of the analyte from 0.000 to 0.01 in steps of 0.00005, for the four sensor arrangements summarized in Table 3. Table S1 outlines some key statistical parameters for the sensitivities observed in figure S3, like mean, standard deviation (S.D.) and coefficient of variation (COV). Additionally, we also give the refractive indices of various layers in Table S2.

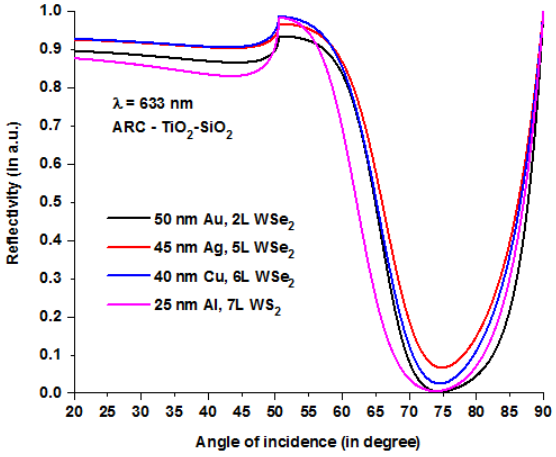

Figure 3. SPR Reflectivity curve

3.2. Electric Field Distribution

Surface plasmons are electron density waves that propagate along the surface of the metal. They also have a component perpendicular to the metallic surface and travel in both directions, into the analyte as well as into the prism. However, the elecric field intensity of these waves decreases as they traverse through the analyte and hence, they are also known as the evanescent field, which means disappearing in nature [26-28]. The field vanishes after they travel about one-half to full wavelength distance. Hence, for a 633 nm incident light source, the field reduces to zero after traveling about 300 nm. The penetration depth, L_p, of this field is defined as the distance at which the field becomes 1/e of its maximum value. In this study, we evaluate the role of four combinations of ARCs (TiO_2-SiO_2, TiO_2-MgF_2, Nb_2O_5-SiO_2 and Nb_2O_5-MgF_2) in increasing the magnitude of the evanescent field. The increase in the evanescent component is due to the excitation of more surface plasmons and thus we get higher sensitivity than the standard Kretschmann configuration. Figure 4 shows the electric field (E_y) variation across the sensor structure for the four different ARCs. We can easily observe the exponentially decreasing nature of the field. We see an increment in the evanescent field (in comparison to the standard Kretschmann configuration) for the different ARCs - 430.21% for TiO_2-SiO_2, 488.58% for TiO_2-MgF_2, 579.00% for Nb_2O_5-SiO_2 and 509.96% for Nb_2O_5-MgF_2. Figure S6 in the supporting information depicts a pictorial representation of the electric field distribution across the sensor surface. The field strength is maximum at the plasmonic metal surface and it decreases exponentially as it traverses towards the sensing medium. The L_p values for the various configurations are: 107.3 nm for standard Au, 105.25 nm for TiO_2-SiO_2, 110.15 nm for TiO_2-MgF_2, 110.34 nm for Nb_2O_5-SiO_2 and 116.8 nm for Nb_2O_5-MgF_2. Since the analyte layer begins at 55.8 nm (50 nm Au + 5 nm Si + 0.8 nm WS_2) from the metal surface, the electric field is still considerably high at this depth. The E_y values at 55.8 nm for the different configurations are: 11398.98 V/m for standard Au, 56486.24 V/m for TiO_2-SiO_2, 63998.98 V/m for TiO_2-MgF_2, 73777.59 V/m for Nb_2O_5-SiO_2 and 68569.97 V/m for Nb_2O_5-MgF_2. Therefore, the electric field values at the TMDC and sensing medium interface are higher for the various ARC configurations as compared to the standard Au. Additionally, biomolecular ligand-analyte interactions that occur within the evanescent wave penetration depth have the ability to change the R.I. of the analyte. Thus, a greater penetration depth of the evanescent field increases the chances of detection of biomolecules.

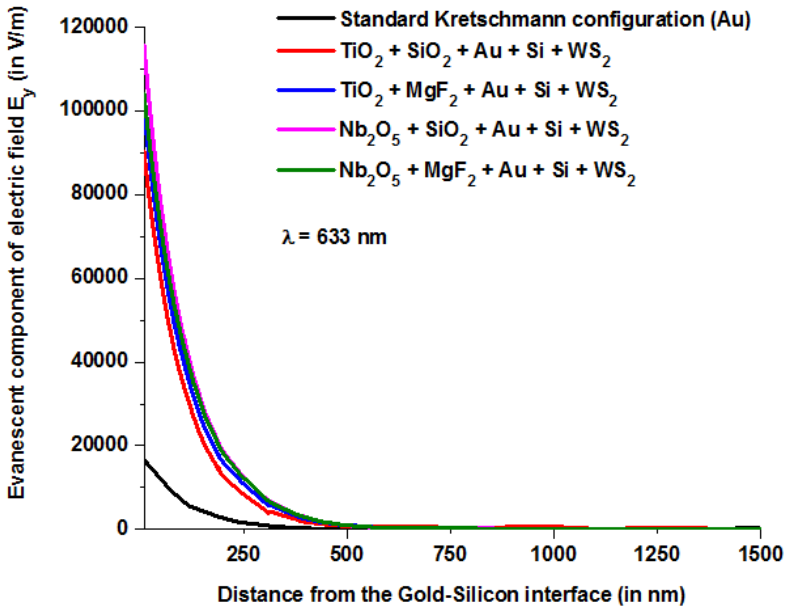

Figure 4. Evanescent field (Ey) variation as a function of distance from the gold surface

3.3. Multi Layered ARC

We take our study further and evaluate the efficacy of multi layered ARCs in further enhancing the sensitivity. Multi layered ARCs contain alternate layers of high and low R.I. materials. We take TiO_2 and SiO_2 as the anti-reflective materials and assess its effect on sensitivity when they are placed suitably in the form of multiple alternating layers. We divide the available thicknesses of TiO_2 and SiO_2 into one-half, one-third and quarter widths to obtain alternate layers of high and low R.I. materials. For four layers of ARC, we use 47.5 nm of TiO_2 followed by 10 nm of SiO_2 and repeat the same. For six layers, we use 32 nm of TiO_2, 7 nm of SiO_2, 32 nm of TiO_2, 7 nm of SiO_2, 31 nm of TiO_2 and 6 nm of SiO_2. For eight layers, we use 23.75 nm of TiO_2 and 5 nm of SiO_2 and repeat it thrice. information depicts variation of sensitivity of multi-layered ARC as a function of number of WS_2 layers. Table 2 shows the simulation results for multi layered ARCs. Figure S7 in the supporting information depicts variation of sensitivity of multi-layered ARC as a function of number of TMDC layers. There is a significant improvement in sensitivity (in comparison to double layered ARC) for Ag, Cu and Al. However, for Au, multi-layered ARC results in a diminishing sensitivity.

Table 2. Summary of simulation results for multi-layered ARC ($\lambda = 633$ nm and $\Delta n_{bio} = 0.005$)

4. Comparison of sensitivity

There have been numerous configurations for SPR sensing that have been proposed before. Our model here makes use of a previously designed TMDC configuration [9] and proposes further sensitivity enhancement in the defined TMDC structure using ARCs. Thus, our basic premise here is to show the effectiveness of ARC in further elevating the sensitivity of pre-defined SPR structures. Biological sensing using SPR technique is quite common nowadays and it has some of its own distinctive advantages. Recently, several works have been reported that use hydrophobic interactions between the TMDC material (predominantly MoS2) and the ligand antibody to detect the corresponding antigen [29-31]. Thus, these MoS2 based SPR sensors can provide easier and faster detection methods without the need of complex functionalization methods required to capture ligand antibody molecules in case of conventional gold based SPR sensors. Thus, our proposed model can be more advantageous in this regard as compared to other earlier proposed designs.

Plasmonic Metal	**Number of layers of ARC TiO_2 – SiO_2**	**TMDC material**	**Sensitivity ($degRIU^{-1}$)**	**Sensitivity Enhancement (in %)**
Au	2	WSe_2 (2L)	284	-
	4		262	N.A.
	6		244	N.A.
	8		242	N.A.
Ag	2	WSe_2 (5L)	190	-
	4		218	14.74
	6		218	14.74
	8		214	12.63
Cu	2	WSe_2 (6L)	214	-
	4		234	9.34
	6		226	5.61
	8		222	3.74
Al	2	WS_2 (7L)	244	-
	4		274	12.30
	6		230	N.A.
	8		220	N.A.

Table 3 below mentions some of these arrangements based on simulation works done by other researchers at incident light wavelength of 633 nm and also gives a comparison of the sensitivity enhancement provided by our model, which is based on the ARC modified Si-TMDC structure.

Table 3. Sensitivity comparison of the ARC modified Si-TMDC structure with other SPR sensing models

Our Predicted Sensitivity (TiO_2-SiO_2-Au-Si-WSe_2) in $degRIU^{-1}$ at 633 nm				**284**
S. No.	**Type of sensor**	**Angular Sensitivity ($degRIU^{-1}$)**	**Active nano-materials in the sensor**	**Enhancement in our proposed sensor (in %)**
1	Kretschmann configuration	74	Au	283.78
2	Si-WS_2, Si-MoS_2 and Si-WSe_2 [9]	147.88, 131.7 and 141.4	Au-Si-TMDC	92.05, 115.64 and 100.84

3	ZnO Graphene TMDC [32]	101.58	ZnO-Au-MoS_2-Graphene	179.58
4	ZnO Graphene [33]	187.43	ZnO-Au-Graphene	51.52
5	TiO_2-SiO_2-MoS_2 [21]	84.09	TiO_2-SiO_2-Au-MoS_2	237.73
6	Bimetal-MoS_2-Graphene [34]	182	Au-MoS_2-Au-Graphene	56.04
7	MoS_2-Graphene-Al [35]	190.83	MoS_2-Al-MoS_2-Graphene	48.82
8	Bimetal-MoS_2-Graphene [36]	229	Au-MoS_2-Ni-Graphene	24.01
9	Bimetal-ZnO-Graphene [37]	222	Au-Graphene-Au-ZnO	27.92
10	Graphene-$BaTiO_3$ [38]	257	Ag-$BaTiO_3$-Graphene	10.50
11	SnSe allotropes [39]	178	Ag-SnSe	59.55
12	Graphene-Si [40]	134.6	Au-Si-Graphene	110.99
13	Graphene-MoS_2[41]	108	Au-MoS_2-Graphene	162.96

5. Conclusion

SPR based bio sensing can give tough competition to other technologies as these can help in the early detection of rare life-threatening diseases, when other conventional detection schemes fail to give reliable results. Hence, it is quite crucial to ensure high sensitivity along with good accuracy, for these sensors. In this work, we demonstrate that by making use double layered ARCs, we can allow more photons to get absorbed and transmitted through the sensing platform, thus allowing greater interaction between itself and the plasmonic metal that leads to enhanced surface plasmon generation, and finally a boost in the sensitivity. With the help of simulation based on the Fresnel's equations for multi-layer reflection, we present a detailed analysis using four kinds of TMDCs (WS_2, MoS_2, WSe_2 and $MoSe_2$), four combinations of ARCs (TiO_2-SiO_2, TiO_2-MgF_2, Nb_2O_5-SiO_2 and Nb_2O_5-MgF_2) and four different plasmonic metals (Au, Ag, Cu and Al). We obtain a sensitivity of 284 degRIU-1 at 633 nm of incident light wavelength with the TiO_2-SiO_2-Au-Si-TMDC configuration. Additionally, we also evaluate the usefulness of multi layered ARCs in further improving the sensitivity, when compared to the double layered ARC arrangement.

Supplementary Information

All additional results are included in the supplementary information.

Acknowledgement

This work was supported by the Singapore National Research Foundation (NRF) and French National Research Agency (ANR), grant number (NRF2017 –ANR002 2DPS).

References

[1] H.H. Nguyen, J. Park, S. Kang, M. Kim. Surface Plasmon Resonance: A Versatile Technique for Biosensor Applications. *Sensors* 2015, vol. 15, no. 5, pp. 10481-10510.

[2] M. Li, S.K. Cushing, N. Wu. Plasmon-enhanced optical sensors: a review. *Analyst* 2015, vol. 140, no. 2, pp. 386-406.

[3] D.S. Wang, S.K. Fan. Microfluidic Surface Plasmon Resonance Sensors: From Principles to Point-of-Care Applications. *Sensors* 2016, vol. 16, no. 8, p. 1175.
[4] A.K. Sharma, B.D. Gupta. On the performance of different bimetallic combinations in surface plasmon resonance based fiber optic sensors. *Journal of Applied Physics* 2007, vol. 101, p. 093111.
[5] N.A. Cinel, S. Bütün, E. Özbay. Electron beam lithography designed silver nano- disks used as label free nano-biosensors based on localized surface plasmon resonance. *Optics Express* 2012, vol. 20, no. 3, pp. 2587-2597.
[6] S. Firdous, S. Anwar, R. Rafya. Development of surface plasmon resonance (SPR) biosensors for use in the diagnostics of malignant and infectious diseases. *Laser Physics Leters* 2018, vol. 15, no. 6, p. 065602.
[7] A.R. Sadrolhosseini, S.A. Rashid, H. Soleimani, S. Shafie, A.S.M. Noor, A. Mohammadi. Application of Surface Plasmon Resonance Sensor with Polypyrrole Chitosan Graphene Oxide layer to Detect the Napropamide. *Journal of Physics: Conference Series* 2018, vol. 1123, no. 1, p. 012016.
[8] Y. Nonobe, T. Yokoyama, Y. kamikubo, S. Yoshida, N. Hisajima, H. Shinohara, Y. Shiraishi, T. Sakurai, T. Tabata. Application of surface plasmon resonance imaging to monitoring G protein-coupled receptor signaling and its modulation in a heterologous expression system. *BMC Biotechnology* 2016, vol. 16, no. 36.
[9] Q. Ouyang, S. Zeng, L. Jiang, L. Hong, G. Xu, X.Q. Dinh, J. Qian, S. He, J. Qu, P. Coquet, K.T. Yong. Sensitivity Enhancement of Transition Metal Dichalcogenides/Silicon Nanostructure-based Surface Plasmon Resonance Biosensor. *Scentific Reports* 2016, vol. 6, no. 1.
[10] J. Hiller, J.D. Mendelsohn, M.F. Rubner. Reversibly erasable nanoporous anti-reflection coatings from polyelectrolyte multilayers. *Nature Materials* 2002, vol. 1, pp. 59-63.
[11] J. Proust, A.L. Fehrembach, F. Bedu, I. Ozerov, N. Bonod. Optimized 2D array of thin silicon pillars for efficient antireflective coatings in the visible spectrum. *Scientific Reports* 2016, vol. 6, 24947.
[12] X. Ye, X. Jiang, J. Huang, F. Geng, L. Sun, X. Zu, W. Wu, W. Zheng. Formation of broadband antireflective and superhydrophilic subwavelength structures on fused silica using one-step self-masking reactive ion etching. *Scientific Reports* 2015, vol. 5, 13023.
[13] Z. Li, J. Lin, Z. Liu, S. Feng, Y. Liu, C. Wang, Y. Liu, S. Yang. Durable Broadband and Omnidirectional Ultra-antireflective Surfaces. *ACS Applied Materials & Interfaces* 2018, vol. 10, no. 46, pp. 40180-40188.
[14] A.R. Parker, H.E. Townley. Biomimetics of photonic nanostructures. *Nature Nanotechnology* 2007, vol. 2, no. 6, pp. 347-353.
[15] M.K. Hedayati, M. Elbahri. Antireflective Coatings: Conventional Stacking Layers and Ultrathin Plasmonic Metasurfaces, A Mini-Review. *Materials* 2016, vol. 9, no. 6, p. 497.
[16] X. Li, J. He. Synthesis of Raspberry-Like SiO_2–TiO_2 Nanoparticles toward Antireflective and Self Cleaning Coatings. *ACS Applied Materials & Interfaces* 2013, vol. 5, no. 11, pp. 5282-5290.
[17] K. Lazarova, M. Vasileva, G. Marinov, T. Babeva. Optical characterization of sol–gel derived Nb_2O_5 thin films. *Optics & Laser Technology* 2014, vol. 58, pp. 114-118.
[18] L. Bao, Z. Ji, H. Wang, R. Chen. Hollow Rodlike MgF_2 with an Ultralow Refractive Index for the Preparation of Multifunctional Antireflective Coatings. *Langmuir* 2017, vol. 33, no. 25, pp. 6240-6247.
[19] A.A. Atta, M.M. El-Nahass, A.M. Hassanien, K.M. Elsabawy, M.M. A El-Raheem, A. Alhuthali, S.E. Alomariy, M.S. Algamdi. Effect of thermal annealing on structural, optical and electrical properties of transparent Nb_2O_5 thin films. *Materials Today Communications* 2017, vol. 13, pp. 112-118.
[20] D. Bernsmeier, J. Polte, E. Ortel, T. Krahl, E. Kemnitz, R. Kraehnert. Antireflective Coatings with Adjustable Refractive Index and Porosity Synthesized by Micelle-Templated Deposition of MgF_2 Sol Particles. *ACS Applied Materials & Interfaces* 2014, vol. 6, no. 22, pp. 19559-19565.
[21] J.B. Maurya, Y.K. Prajapati, V. Singh, J.P. Saini. Sensitivity enhancement of surface plasmon resonance sensor based on graphene–MoS_2 hybrid structure with TiO_2–SiO_2 composite layer. *Applied Physics A* 2015, vol. 121, no. 2, pp. 525-533.
[22] J.R. Devore. Refractive indices of rutile and sphalerite. *Journal of Optical Society of America* 1951, vol. 41, no. 6, pp. 416-419.
[23] I.H. Malitson. Interspecimen comparison of the refractive index of fused silica. *Journal of Optical Society of America* 1965, vol. 55, no. 10, pp. 1205-1209.
[24] L. Gao, F. Lemarchand, M. Lequime. Exploitation of multiple incidences spectrometric measurements for thin film reverse engineering. *Optics Express* **2012**, vol. 20, no. 14, pp. 15734-15751.

[25] M.J. Dodge. Refractive properties of magnesium fluoride. *Applied Optics* **1984**, vol. 23, no. 12, pp. 1980-1985.
[26] C. Schlachter, F. Lisdat, M. Frohme, V.A. Erdmann, Z. Konthur, H. Lehrach, J. Glökler. Pushing the detection limits: The evanescent field in surface plasmon resonance and analyte-induced folding observation of long human telomeric repeats. *Biosensors and Bioelectronics* 2012, vol. 31, no. 1, pp. 571-574.
[27] J. Renger, S. Grafström, L.M. Eng. Evanescent wave scattering and local electric field enhancement at ellipsoidal silver particles in the vicinity of a glass surface. *Journal of Optical Society of America* 2004, vol. 21, no. 7, pp. 1362-1367.
[28] S. Ekgasit, C. Thammacharoen, F. Yu, W. Knoll. Evanescent Field in Surface Plasmon Resonance and Surface Plasmon Field-Enhanced Fluorescence Spectroscopies. *Analytical Chemistry* 2004, vol. 76, no. 8, pp. 2210-2219.
[29] S. Kaushik, U.K. Tiwari, A. Deep, R.K. Sinha. Two-dimensional transition metal dichalcogenides assisted biofunctionalized optical fiber SPR biosensor for efficient and rapid detection of bovine serum albumin. Sci. Rep. 2019, vol. 9, 6987.
[30] S. Kaushik, U.K. Tiwari, S.S. Pal, R.K. Sinha. Rapid detection of Escherichia coli using fiber optic surface plasmon immunosensor based on biofunctionalized Molybdenum disulfide (MoS2) nanosheets. Biosensors and Bioelectronics 2019, vol. 126, pp. 501-599.
[31] W. Nie, Q. Wang, X. Yang, H. Zhang, Z. Li, L. Gao, Y. Zheng, X. Liu, K. Wang. High sensitivity surface plasmon resonance biosensor for detection of microRNA based on gold nanoparticles-decorated molybdenum sulfide. Analytica Chimica Acta 2017, vol. 993, pp. 55-62.
[32] A.S. Kushwaha, A. Kumar, R. Kumar, S.K. Srivastava. A study of surface plasmon resonance (SPR) based biosensor with improved sensitivity. *Photonics & Nanostructures – Fundamentals & Applications* **2018**, vol. 31, pp. 99-106.
[33] A.S. Kushwaha, A. Kumar, R. Kumar, M. Srivastava, S.K. Srivastava. Zinc oxide, gold and graphene-based surface plasmon resonance (SPR) biosensor for detection of pseudomonas like bacteria: A comparative study. *Optik – International Journal for Light and Electron Optics* 2018, vol. 172, pp. 697-707.
[34] Z. Lin, L. Jiang, L. Wu, J. Guo, X. Dai, Y. Xiang, D. Fan. Tuning and Sensitivity Enhancement of Surface Plasmon Resonance Biosensor With Graphene Covered Au-MoS_2-Au Films. *IEEE Photonics Journal* 2016, vol. 8, no. 6, p. 4803308
[35] L. Wu, Y. Jia, L. Jiang, J. Guo, X. Dai, Y. Xiang, D. Fan. Sensitivity Improved SPR Biosensor Based on the MoS_2/Graphene–Aluminum Hybrid Structure. *Journal of Lightwave Technology* **2017**, vol. 35, no. 1, pp. 82-87.
[36] A. Nisha, P. Maheshwari, P.M. Anbarasan, K.B. Rajesh, Z. Jaroszewicz. Sensitivity enhancement of surface plasmon resonance sensor with 2D material covered noble and magnetic material (Ni). *Optical and Quantum Electronics* 2019, vol. 51, no. 19.
[37] L. Liu, W. Du, D. Wu, K. Jiao, L. Jiao, M. Wang, F. Xia, W. Kong, M. Yun. Sensitivity enhancement of surface plasmon resonance biosensor with graphene sandwiched between two metal films. *Proc. Of SPIE Plasmonics: Design, Materials, Fabrication, Characterization, and Applications XVI, 1072224* 2018, vol. 10722.
[38] P. Sun, M. Wang, L. Liu, L. Jiao, W. Du, F. Xia, M. Liu, W. Kong, L. Dong, M. Yun. Sensitivity enhancement of surface plasmon resonance biosensor based on graphene and barium titanate layers. *Applied Surface Science* 2019, vol. 475, pp. 342-347.
[39] X. Dai, Y. Liang, Y. Zhao, S. Gan, Y. Jia, Y. Xiang. Sensitivity Enhancement of a Surface Plasmon Resonance with Tin Selenide (SnSe) Allotropes. *Sensors* 2019, vol. 19, no. 1, p. 173.
[40] R. Verma, B.D. Gupta, R. Jha. Sensitivity enhancement of a surface plasmon resonance based biomolecules sensor using graphene and silicon layers. *Sensors and Actuators B: Chemical* 2011, vol. 160, no. 1, pp. 623-631.
[41] S. Zeng, S. Hu, J. Xia, T. Anderson, X.Q. Dinh, X.M. Meng, P. Coquet, K.T. Yong. Graphene–MoS_2 hybrid nanostructures enhanced surface plasmon resonance biosensors. *Sensors and Actuators B: Chemical* 2015, vol. 207, pp. 801-810.